Modeling elastic wave propagation in fluid-filled boreholes drilled in nonhomogeneous media: BEM – MLPG versus BEM-FEM coupling

A. Tadeu[1,2] , A. Romero[3], P. Stanak[4], J. Sladek[5], V. Sladek[5], P. Galvín[3], J. Antonio[2]

[1] ITeCons - Institute for Research and Technological Development in Construction, Energy, Environment and Sustainability, Rua Pedro Hispano, 3030-289 Coimbra, Portugal

[2] ADAI - LAETA, Department of Civil Engineering, University of Coimbra, Pólo II, Rua Luís Reis Santos, 3030-788 Coimbra, Portugal

[3] Escuela Técnica Superior de Ingeniería, Universidad de Sevilla, Camino de los Descubrimientos, 41092 Sevilla, Spain

[4] On leave from Institute of Construction and Architecture, Slovak Academy of Sciences, 84503 Bratislava, Slovakia

[5] Institute of Construction and Architecture, Slovak Academy of Sciences, 84503 Bratislava, Slovakia

corresponding author: tadeu@itecons.uc.pt

Abstract:
The efficiency of two coupling formulations, the boundary element method (BEM) - meshless local Petrov-Galerkin (MLPG) versus the BEM- finite element method (FEM), used to simulate the elastic wave propagation in fluid-filled boreholes generated by a blast load, are compared. The longitudinal geometry is assumed to be invariant in the axial direction (2.5D formulation). The material properties in the vicinity of the borehole are assumed to be nonhomogeneous as a result of the construction process and the ageing of the material. In both models, the BEM is used to tackle the propagation within the fluid domain inside the borehole and the unbounded homogeneous domain. The MLPG and the FEM are used to simulate the confined, damaged, nonhomogeneous, surrounding borehole, thus utilizing the advantages of these methods in modeling nonhomogeneous bounded media. In both numerical techniques the coupling is accomplished directly at the nodal points located at the common interfaces. Continuity of stresses and displacements is imposed at the solid-solid interface, while continuity of normal stresses and displacements and null shear stress are prescribed at the fluid-solid interface. The performance of each coupled BEM-MLPG and BEM-FEM approach is determined using referenced results provided by an analytical solution developed for a circular multi-layered subdomain. The comparison of the coupled techniques is evaluated for different excitation frequencies, axial wavenumbers and degrees of freedom (nodal points).

Keywords: wave propagation, fluid-solid interaction, damaged zone, coupling techniques

1. Introduction

Numerical simulations of various physical phenomena have become an inseparable part of engineering design and scientific research in almost all disciplines. Numerical analysis of partial differential equations using computer modeling has gained special attention. Once validated, numerical models enable advanced design, optimization and control of new products, processes or development of new research theories. Elastic wave propagation in nonhomogeneous media is a significant research topic in various fields of engineering and science. Several numerical tools have been developed for elastic wave propagation analysis, including the well-known boundary element method (BEM) [1-3], the finite element method (FEM) [4-5], the hybrid numerical method [6], and meshless methods such as the meshless local Petrov-Galerkin method (MLPG) [7-9].

The BEM is particularly useful for problems involving large scale unbounded domains since the far field boundary conditions are automatically satisfied. However, the BEM can only be used for analyzing more general geometries and media when the relevant fundamental solutions or Green's functions required in the boundary integral equation are known. But for problems involving nonhomogenous media where the elastic material properties vary the fundamental solution is generally unavailable in the closed form. The BEM also requires the correct integration of the resulting singular and hypersingular integrals to guarantee its efficiency. Domain discretization methods such as the FEM or MLPG also have some disadvantages, related mainly to discretization of complex and large geometries. The coarse discretization might restrict the models to low frequencies if we wish to maintain accuracy. The meshless methods have their own disadvantages and limitations. The interpolations and the algorithm implementation of meshless methods tend to be computationally expensive and these methods can be inefficient for problems with infinite and semi-infinite domains [10].

Evaluation of the efficiency, convergence and accuracy of different numerical methods and approaches is an inevitable part of numerical modeling. A patch test was developed to assess the different elements used in FEM [11]. Satisfaction of the patch test can be considered a necessary and sufficient condition of convergence of FEM [12]. Convergence analysis and asymptotic error estimates of BEM were performed by Schmidt and Strese [13] for a mixed boundary value problem. Vavourakis, Sellountos and Polyzos [14] provided a detailed comparative study of five different MLPG (LBIE) formulations and concluded that derivatives of shape functions decrease solution accuracy and that a uniform distribution of nodes gives the best results. The effect of nodal distribution on the accuracy of MLPG formulations was also presented in [15]. Sladek et al. [16] compared the stability, convergence of accuracy and cost efficiency of four meshless formulations for the solution of boundary value problems in nonhomogeneous elastic solids. Application of the MLPG method to the analysis of a broad range of scientific problems is summarized in the review article by Sladek et al. [17].

In recent years, increased attention has been given to the development of theoretical and numerical models to simulate systems that incorporate both homogeneous and nonhomogeneous media and account for the interaction between them. Elastic wave propagation in nonhomogeneous media is a significant research topic in certain fields of engineering and science including geotechnics, earthquake engineering and non-destructive

testing. It is also of interest in acoustic wave propagation and thermal diffusion problems. In many cases, the nonhomogeneous inclusions are placed or buried in a homogeneous surrounding medium. The analysis of wave propagation phenomena in elastic media and the interaction between different solid heterogeneous inclusions and different host domains has been an important research subject. However, since no single numerical method can properly handle such computational problems because of their increasing complexity, the idea of combining different numerical methods and computational techniques emerged, aiming to utilize their individual advantages while at the same time minimizing their disadvantages. That is why many researchers have been interested in coupling various numerical methods. The MLPG method has been coupled with FEM to tackle elasticity problems [18], potential problems [19] and electromagnetic field computations [20]. FEM was coupled with BEM in [21-23]. Other examples include combining BEM with the method of fundamental solutions (MFS) [24], BEM with meshless Kansa's method [25], FEM with EFG method [26], FEM with MFS [27] and MFS with MLPG [28]. Tadeu et al. [29] used a coupled BEM-MLPG approach for the thermal analysis of nonhomogeneous media. A similar technique was also used for the acoustic analysis of nonhomogeneous inclusions [30]. Elastic wave propagation in nonhomogeneous media was examined in [31]. Direct coupling with the use of a moving least squares (MLS) approximation scheme was employed. This direct coupling method does not require the concept of overlapping "double nodes" for mutual BEM-MLPG coupling. Iterative coupling can be used instead of direct coupling. In the iterative coupling approach, each subdomain of the global model is analyzed separately as an uncoupled model, and the variables are successively renewed at the common interfaces until convergence is achieved [32].

Researchers have been studying the accuracy and convergence of various coupling formulations. Wendland [33] presents a survey on the corresponding current mathematical analysis in the framework of asymptotic convergence and error estimates of combined BEM and FEM. Godinho and Soares [32] performed a numerical analysis of interacting acoustic–elastodynamic models using the BEM and the MFS to model the acoustic sub-domains, while the FEM, the collocation method and the MLPG method were used to model the elastodynamic sub-domains. The performance and advantages of these methods were investigated.

Because of the range of modeling and solution possibilities, it could be useful to determine the efficiency and accuracy of various coupling procedures for a given problem. The interaction between a fluid and the heterogeneous material buried in elastic host media are important research issues in civil, geophysical or oil-drilling engineering. Wave propagation in fluid-filled boreholes from sources inside and outside the borehole has been studied by many researchers [34-38] and thus may be regarded as a good study case for comparing coupling approaches.

In this paper two numerical methods are utilized to discretize the nonhomogeneous elastic subdomains and one for homogeneous elastic and fluid subdomains, as recently analyzed in [39]. A two-and-a-half-dimensional (2.5D) approach [40] is applied to this problem, assuming longitudinally invariant structures. The numerical analysis of fluid-solid coupled

systems is a complex task, requiring the proper treatment of subdomains in which different physical phenomena are involved. In this context, the BEM is used to discretize the fluid and homogeneous elastic subdomains and the FEM and a meshless method based on the MLPG are used to model the nonhomogeneous elastic subdomain. The BEM-FEM and BEM-MLPG coupled techniques are thus considered.

The two coupled approaches are tested against the results provided by an analytical solution developed for a circular multi-layered subdomain, in which the material properties within the circular nonhomogeneous region are assumed to vary in the radial direction. The continuity conditions for the displacements and tractions are specified for nodes at the interface between the unbounded solid and the damaged solid medium. Four boundary conditions must be prescribed at the interface between the fluid and solid phase: continuity of normal stresses and displacements, and null shear stress. The mutual direct coupling between the BEM and the MLPG is accomplished by inserting the coupling conditions discretized by the MLS scheme into the boundary integral equations for displacements and fluid pressure. For the BEM-FEM coupling, the element shape functions are used to discretize the coupling conditions. The imposition of these conditions leads to a system of equations that can be solved for the nodal solid displacements and fluid pressures. All calculations are performed in the frequency domain. Final responses in the time domain may be obtained by means of the fast inverse Fourier transformation. By using these different numerical approaches we are able to assess the relative advantages and disadvantages of each coupling methodology. This allows the effectiveness and accuracy of these different methodologies to be compared when analyzing a given fluid-structure interaction coupled problem.

2. Governing equations for 2.5D analysis

Elastic wave propagation in a nonhomogeneous isotropic medium is governed by the following well-known equilibrium equation:

$$\sigma_{ij,j}\left(\mathbf{x},t\right)=\rho\ddot{u}_i\left(\mathbf{x},t\right) \tag{1}$$

where σ_{ij} is the stress tensor, u_i are mechanical displacements and ρ is the mass density. A comma followed by an index denotes partial differentiation with respect to the coordinate associated with the index $i, j=1,2,3$. The dots over the quantity indicate the derivative with respect to time t.

Applying the Fourier transform $F\left(\omega\right)=\int_{-\infty}^{\infty} f\left(t\right)e^{\mathrm{i}\omega t}dt$ to equation (1) yields the transformation to frequency domain as:

$$\sigma_{ij,j}\left(\mathbf{x},\omega\right)=-\omega^2\rho u_i\left(\mathbf{x},\omega\right) \tag{2}$$

where ω is the angular frequency and a dependence of the type $e^{i\omega t}$ is implicit.

Stress tensor σ_{ij} is defined by means of Hooke's law as

$$\sigma_{ij} = C_{ijkl}\varepsilon_{kl} \tag{3}$$

where C_{ijkl} and ε_{kl} are the stress-strain matrix in an isotropic medium and elastic strain tensor defined as follows:

$$C_{ijkl} = \lambda\delta_{ij}\delta_{kl} + \mu\left(\delta_{ik}\delta_{jl} + \delta_{il}\delta_{jk}\right),\ \varepsilon_{kl} = \frac{1}{2}\left(u_{k,l} + u_{l,k}\right) \tag{4}$$

where $\lambda,\ \mu$ are the Lame material constants and δ_{ij} is the Kronecker delta symbol. $\lambda,\ \mu$ depend on the shear c_s and dilatational c_p wave velocities according to

$$c_s = \sqrt{\frac{\mu}{\rho}},\ c_p = \sqrt{\frac{\lambda + 2\mu}{\rho}} \tag{5}$$

Numerous engineering problems can be characterized by the continuous nonhomogeneity of isotropic material with varying Young's modulus $E(\mathbf{x})$, while the Poisson ratio ν is assumed to be constant. Spatially varying the Lame constants can be defined as:

$$\mu(\mathbf{x}) = \frac{E(\mathbf{x})}{2(1+\nu)},\ \lambda(\mathbf{x}) = \frac{E(\mathbf{x})\nu}{(1+\nu)(1-2\nu)} \tag{6}$$

One can see that by omitting the component notation of the vector quantities, Eq. (2) can be easily transformed into the following well-known governing equation for the elastic wave propagation in the frequency domain:

$$\nabla\left([\lambda + 2\mu]\nabla\cdot\mathbf{u}\right) - \nabla\times\left(\mu\nabla\times\mathbf{u}\right) + 2\left(\nabla\mathbf{u}\cdot\nabla\mu\right) = -\omega^2\rho\mathbf{u} \tag{7}$$

In the 2.5D analysis, the geometry of the media is constant in one direction and the load can be 3D. The response is expressed by applying a spatial Fourier transform in that direction (usually the z-axis - index 3).

Taking Eq. (2), we can separate the third component (thus $\alpha = 1,2$) as

$$\sigma_{i\alpha,\alpha}(\mathbf{x},\omega) + \sigma_{i3,3}(\mathbf{x},\omega) = -\omega^2\rho u_i(\mathbf{x},\omega) \tag{8}$$

Performing the spatial Fourier transformation $\tilde{f}(k_z) = \int_{-\infty}^{\infty} f(z)e^{-\mathrm{i}k_z z}dz$ on Eq. (8) we obtain the governing equations for Fourier transforms:

$$\tilde{\sigma}_{i\alpha,\alpha}(\mathbf{x},k_z,\omega) + \mathrm{i}k_z\tilde{\sigma}_{i3}(\mathbf{x},k_z,\omega) = -\omega^2\rho\tilde{u}_i(\mathbf{x},k_z,\omega) \tag{9}$$

where k_z is the axial wave number, $\mathbf{x} \equiv (x,\ y)$ and a dependence of the type $e^{-\mathrm{i}k_z z}$ is again implicit.

For a fluid medium, the wave propagation is governed by the well-known Helmholz equation,

$$\nabla^2 p(\mathbf{x},\omega) + \omega^2 / c_p{}^2 \; p(\mathbf{x},\omega) = 0 \tag{10}$$

where $p(\mathbf{x}, \omega)$ represents the pressure field. Again performing the spatial Fourier transformation $\tilde{f}(k_z) = \int_{-\infty}^{\infty} f(z) e^{-ik_z z} dz$ on Eq. (10), the governing equation for Fourier transforms is obtained as

$$\left(\frac{\partial^2}{\partial x^2} + \frac{\partial^2}{\partial y^2} \right) \tilde{p}(\mathbf{x}, k_z, \omega) + (\omega^2 / c_p{}^2 - k_z^2) \tilde{p}(\mathbf{x}, k_z, \omega) = 0 \tag{11}$$

This equation will be used in the analysis of the fluid-filled bounded domain, as shown in the next sections.

3. Numerical formulations

Let us now consider a two dimensional fluid-filled borehole Ω_1 with a damaged nonhomogeneous zone Ω_2, having density ρ_2, buried in a homogeneous unbounded elastic domain Ω_3 with density ρ_3, as shown in Figure 1. c_{p_m}, $m = 1,2,3$, is the longitudinal wave velocity, and the shear wave velocity of each medium $n = 2,3$ is denoted by c_{s_n}. Interfaces between the media are denoted as Γ_1 and Γ_2.

This problem is chosen to evaluate the performance of a coupling of the BEM and the MLPG vs. the BEM and the FEM. The purpose is to exploit the advantages of each numerical method for the appropriate part of the problem. MLPG and FEM is used for the Ω_2 domain since it is best suited to analyzing nonhomogeneous media. The BEM, meanwhile, is used to analyze the Ω_1 and Ω_3 domains, which have homogeneous material properties. Domain Ω_2 is discretized by nodal points uniformly distributed over the analyzed domain, while domains Ω_1 and Ω_3 are discretized by constant boundary elements at Γ_1 and Γ_2 as indicated in Figure 1.

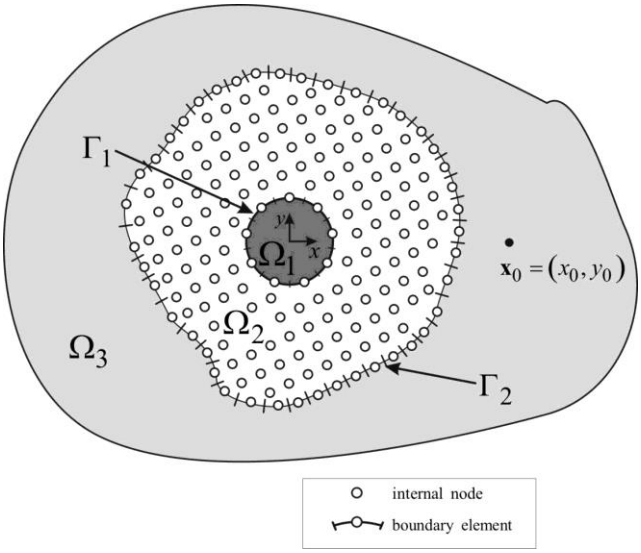

Figure 1: Problem definition

3.1. BEM formulation

3.1.1 BEM formulation for domain Ω_3

The BEM solution of Eq. (2) for the 2.5D problem in medium Ω_3, bounded by surface Γ_2 and subjected to an incident displacement field u_i^{inc} is presented next. By applying the reciprocity theorem we obtain the following boundary integral equations:

$$p_{ij}\tilde{u}_j(\mathbf{x}_0, k_z, \omega) = \int_{\Gamma_2} \tilde{t}_j(\mathbf{x}, \mathbf{n}_n, k_z, \omega) G_{ij}(\mathbf{x}, \mathbf{x}_0, k_z, \omega) d\Gamma - \\ -\int_{\Gamma_2} \tilde{u}_j(\mathbf{x}, k_z, \omega) H_{ij}(\mathbf{x}, \mathbf{x}_0, \mathbf{n}_n, k_z, \omega) d\Gamma + \tilde{u}_i^{inc}(\mathbf{x}_0, \mathbf{x}_s, k_z, \omega) \quad (12)$$

In this equation, the coefficient p_{ij} is equal to $\delta_{ij}/2$ when the boundary Γ_2 is smooth, $\tilde{u}_j(\mathbf{x}, k_z, \omega)$ represents the displacement field at $\mathbf{x} = (x, y)$, $\tilde{t}_j(\mathbf{x}, \mathbf{n}_n, k_z, \omega)$ specifies nodal tractions in direction *j* on the boundary at $\mathbf{x} = (x, y)$, $\mathbf{n}_n$ is the unit outward normal vector on the boundary Γ_2 at (x, y) defined by $\mathbf{n}_n = (\cos\theta_n, \sin\theta_n)$. $G_{ij}(\mathbf{x}, \mathbf{x}_0, k_z, \omega)$ and $H_{ij}(\mathbf{x}, \mathbf{x}_0, \mathbf{n}_n, k_z, \omega)$ correspond to the fundamental solutions for displacement and traction (Green's functions) for the elastic medium in Ω_3, in direction *j* at $\mathbf{x}$, caused by a unit point load in direction *i* applied at the collocation point $\mathbf{x}_0 = (x_0, y_0)$. The derivation of the Green's functions for 2.5D problems can be found in [31,40]. $\tilde{u}_i^{inc}(\mathbf{x}_0, \mathbf{x}_s, k_z, \omega)$ represents the incident displacement field in direction *i* at $\mathbf{x}_0$ with the source located at $\mathbf{x}_s = (x_s, y_s)$.

The boundary Γ_2 is then discretized into N_{be}^2 constant boundary elements, with each having one nodal point. Each of the three loads (aligned in the horizontal, vertical and z directions) is applied sequentially to all nodal points to obtain $3N_{be}^2$ equations.

3.1.2 BEM formulation for domain Ω_1

The BEM is also used to analyze the fluid-filled domain Ω_1 placed within the nonhomogeneous domain Ω_2 in the same way as described in the previous section. However, in this case the integral equation for the pressure $\tilde{p}$ is written as:

$$c\tilde{p}\left(\mathbf{x}_0,k_z,\omega\right)=-\rho_1\omega^2\int_{\Gamma_1}\tilde{u}_{nf}\left(\mathbf{x},k_z,\omega\right)G_f\left(\mathbf{x},\mathbf{x}_0,k_z,\omega\right)d\Gamma+ \\ +\int_{\Gamma_1}\tilde{p}\left(\mathbf{x},k_z,\omega\right)H_f\left(\mathbf{x},\mathbf{x}_0,\mathbf{n}_n,k_z,\omega\right)d\Gamma \tag{13}$$

In this equation, c is equal to 0.5 when the boundary Γ_1 is smooth, $\tilde{u}_{nf}\left(\mathbf{x},k_z,\omega\right)$ represents the normal displacement field at $\mathbf{x}=\left(x,y\right)$ on the boundary, $\tilde{p}\left(\mathbf{x},k_z,\omega\right)$ specifies the pressure on the boundary at $\mathbf{x}=\left(x,y\right)$ and the subscript f is used for fluid. $G_f\left(\mathbf{x},\mathbf{x}_0,k_z,\omega\right)$ and $H_f\left(\mathbf{x},\mathbf{x}_0,\mathbf{n}_n,k_z,\omega\right)$ are the fundamental solutions for pressure and displacement:

$$G_f\left(\mathbf{x},\mathbf{x}_0,k_z,\omega\right)=-\frac{\mathrm{i}}{4}H_0\left(k_{c_{p1}}\sqrt{\left(x-x_0\right)^2+\left(y-y_0\right)^2}\right) \tag{14}$$

$$H_f\left(\mathbf{x},\mathbf{x}_0,\mathbf{n}_n,k_z,\omega\right)=\frac{\mathrm{i}k_{c_{p1}}}{4}H_1\left(k_{c_{p_1}}\sqrt{\left(x-x_0\right)^2+\left(y-y_0\right)^2}\right)\frac{\partial r}{\partial n} \tag{15}$$

where $H_n\left(...\right)$ are second kind Hankel functions of the order n and $k_{c_{p1}}=\sqrt{\omega^2/{c_{p_1}}^2-k_z^2}$ is assumed with $\mathrm{Im}\left(k_{c_{p_1}}\right)<0$.

The boundary Γ_1 is then discretized into N_{be}^1 constant boundary elements, each with one nodal point. The necessary integrations over the boundary elements can generally be performed by means of standard Gaussian quadrature. To ensure that the method is accurate, when the loaded element coincides with the integrated element the resulting singular integration should be performed analytically, following the expressions in [41, 42], for example.

3.2. BEM – MLPG

3.2.1 MLPG formulation for domain Ω_2

The MLPG technique [7] was chosen for the meshless analysis of elastic wave propagation in the domain Ω_2, assuming the MLS approximation for the definition of the trial functions and the Heaviside unit step function as a test function in each local subdomain Ω_S. Instead of writing the global weak form, the MLPG is based on the local weak form of the governing equations. The shape of the local integration domain Ω_S can be arbitrary, and we adopted a cylindrical shape aligned in the longitudinal z=3 direction. Since the problem is assumed infinite in the longitudinal direction, the volume integral can be decomposed as an integral over the z-coordinate and the cross section of cylinder Ω_S. The local integration domain Ω_S is shown in Fig. 2 for the 2D example.

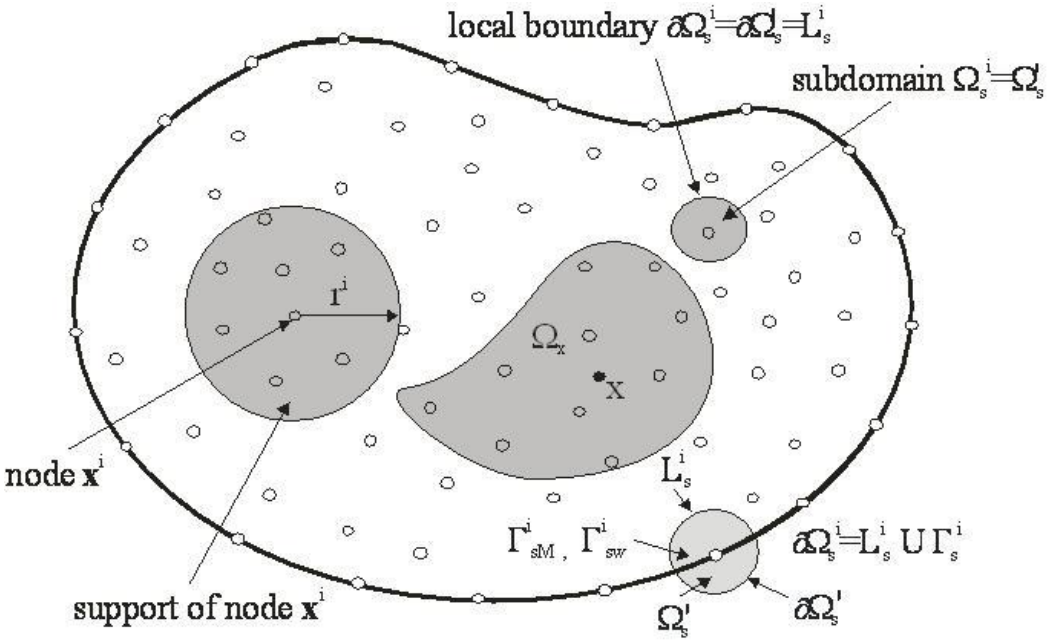

Figure 2: Local boundaries for the weak formulation, the Ω_x domain for MLS approximation of the trial function, and the support area of weight function around a node.

The local weak form of Eq. (9) is then written over each subdomain Ω_S as:

$$\int_{\Omega_S} \left[\tilde{\sigma}_{i\alpha,\alpha}(\mathbf{x},k_z,\omega) + \mathrm{i}k_z \tilde{\sigma}_{i3}(\mathbf{x},k_z,\omega) + \omega^2 \rho \tilde{u}_i(\mathbf{x},k_z,\omega) \right] w^*(\mathbf{x})\, d\Omega = 0 \tag{16}$$

Applying the Gauss divergence theorem to the left-hand side integral in Eq. (16) leads to:

$$\begin{aligned} &\int_{\partial\Omega_S} n_\alpha(\mathbf{x}) \tilde{\sigma}_{i\alpha}(\mathbf{x},k_z,\omega) w^*(\mathbf{x})\, d\Gamma - \int_{\Omega_S} \tilde{\sigma}_{i\alpha}(\mathbf{x},k_z,\omega) w^*_{,\alpha}(\mathbf{x})\, d\Omega \\ &+ \int_{\Omega_S} \left[\mathrm{i}k_z \tilde{\sigma}_{i3}(\mathbf{x},k_z,\omega) + \omega^2 \rho \tilde{u}_i(\mathbf{x},k_z,\omega) \right] w^*(\mathbf{x})\, d\Omega = 0 \end{aligned} \tag{17}$$

where $n_j(\mathbf{x})$ is the unit normal vector and $\partial\Omega_S$ is the boundary of the subdomain Ω_S. Assuming the Heaviside unit step function for the test function,

$$w^*(\mathbf{x}) = \begin{cases} 1 \text{ at } \mathbf{x} \in (\Omega_s \cup \partial\Omega_s) \\ 0 \text{ at } \mathbf{x} \notin (\Omega_s \cup \partial\Omega_s) \end{cases} \tag{18}$$

the following local integral equation (LIE) is finally obtained:

$$\int_{\partial\Omega_S} n_\alpha(\mathbf{x})\tilde{\sigma}_{i\alpha}(\mathbf{x},k_z,\omega)\,d\Gamma + \int_{\Omega_S}\left[\mathrm{i}k_z\tilde{\sigma}_{i3}(\mathbf{x},k_z,\omega) + \omega^2\rho\tilde{u}_i(\mathbf{x},k_z,\omega)\right]d\Omega = 0 \tag{19}$$

The integrand in the first boundary integral in Eq. (19) can be identified as the Fourier transform of the traction vector $\tilde{t}_i(\mathbf{x},k_z,\omega) = n_\alpha(\mathbf{x})\tilde{\sigma}_{i\alpha}(\mathbf{x},k_z,\omega)$.

The Fourier transform of the stress tensor σ_{ij} in the axial z-direction can be expressed in terms of the Fourier transforms of displacements for $\alpha,\beta,\gamma = 1,2$ as:

$$\tilde{\sigma}_{i\alpha} = \delta_{i\beta}\left[\lambda\delta_{\alpha\beta}\left(\tilde{u}_{\gamma,\gamma} + \mathrm{i}k_z\tilde{u}_3\right) + \mu\left(\tilde{u}_{\alpha,\beta} + \tilde{u}_{\beta,\alpha}\right)\right] + \delta_{i3}\mu\left(\tilde{u}_{3,\alpha} + \mathrm{i}k_z\tilde{u}_\alpha\right) \quad , \quad \left(\sum_{\beta}\right) \tag{20}$$

$$\tilde{\sigma}_{i3} = \delta_{i\beta}\mu\left(\tilde{u}_{3,\beta} + \mathrm{i}k_z\tilde{u}_\beta\right) + \delta_{i3}\left[\lambda\tilde{u}_{\gamma,\gamma} + \mathrm{i}k_z\left(\lambda+2\mu\right)\tilde{u}_3\right], \quad \left(\sum_{\beta}\right) \tag{21}$$

Thus, LIE (19) for $i = \beta$ takes the form:

$$\int_{\partial\Omega_S}\left[\lambda n_\beta\left(\tilde{u}_{\gamma,\gamma} + \mathrm{i}k_z\tilde{u}_3\right) + \mu n_\alpha\left(\tilde{u}_{\alpha,\beta} + \tilde{u}_{\beta,\alpha}\right)\right]d\Gamma + \int_{\Omega_S}\left[\mathrm{i}k_z\mu\tilde{u}_{3,\beta} + \left(\omega^2\rho - k_z^2\mu\right)\tilde{u}_\beta\right]d\Omega = 0 \tag{22}$$

while for $i = 3$ we obtain:

$$\int_{\partial\Omega_S}\mu n_\alpha\left[\tilde{u}_{3,\alpha} + \mathrm{i}k_z\tilde{u}_\alpha\right]d\Gamma + \int_{\Omega_S}\left[\mathrm{i}k_z\lambda\tilde{u}_{\gamma,\gamma} + \left(\omega^2\rho - k_z^2\left(\lambda+2\mu\right)\right)\tilde{u}_3\right]d\Omega = 0 \tag{23}$$

We have formulated the MLPG method using the moving least-squares method (MLS) to approximate the displacement field over a number of nodal points randomly distributed over the domain Ω_2 and the interfaces Γ_1 and Γ_2, by using a set of nodes across the domain of influence. According to the MLS method [7], the approximation $\tilde{\mathbf{u}}^h(\mathbf{x},k_z,\omega)$ of the displacement field $\tilde{\mathbf{u}}(\mathbf{x},k_z,\omega)$ over a number of randomly located nodes $\{\mathbf{x}^i\}$, $i = 1,2,...N$, is given by the following equation:

$$\tilde{\mathbf{u}}(\mathbf{x},k_z,\omega) \cong \tilde{\mathbf{u}}^h(\mathbf{x},k_z,\omega) = \sum_{i=1}^{N}\phi^i(\mathbf{x})\hat{\mathbf{u}}^i(k_z,\omega). \tag{24}$$

where $\hat{\mathbf{u}}^i(k_z,\omega)$ are so called fictitious nodal values of approximated field [7] and $\phi^i(\mathbf{x})$ is the MLS shape function. The MLS shape function is defined using the monomial basis vector of order *m*=6 (for the 2D case), with quadratic polynomials.

For the approximation of derivatives of displacements (strains), we can use

$$\tilde{\mathbf{u}}_{,\alpha}(\mathbf{x},k_z,\omega)=\sum_{i=1}^{N}\phi^i_{,\alpha}(\mathbf{x})\hat{\mathbf{u}}^i\left(k_z,\omega\right), \tag{25}$$

The number of nodes N used for the approximation is determined by the weight function $w^i(\mathbf{x})$. A 4th order spline-type weight function is applied in the present work as follows:

$$w^i(\mathbf{x})=\begin{cases}1-6\left(\dfrac{d^i}{r^i}\right)^2+8\left(\dfrac{d^i}{r^i}\right)^3-3\left(\dfrac{d^i}{r^i}\right)^4, & 0\le d^i\le r^i\\ 0, & d^i\ge r^i\end{cases}, \tag{26}$$

where $d^i=\left\|\mathbf{x}-\mathbf{x}^i\right\|$ and r^i is the size of the support domain. In fact, it is the number of nodes lying in the support domain with radius r^i which determines the value of N. It is seen that the C^1-continuity is ensured over the entire domain, and therefore the continuity of gradients of the approximated displacement fields is satisfied. In the MLS approximation, the rate of convergence of the solution may depend upon the nodal distance as well as the size of the support domain [43]. It should be noted that a smaller subdomain size could induce larger oscillations in the nodal shape functions [7]. A necessary condition for a regular MLS approximation is that at least m weight functions are non-zero (i.e. $N\ge m$) for each sample point $\mathbf{x}\in\Omega_2$. This condition determines the size of the support domain.

Discretized LIEs are obtained by substitution of expressions (24) and (25) for spatial MLS approximations of displacements and their derivatives into Eqs. (22) and (23) considered for each subdomain $\Omega_s^c\subset\Omega_2$ as:

$$\begin{aligned}&\sum_{a=1}^{N}\hat{u}_\gamma{}^a\left(k_z,\omega\right)\left\{\int_{\partial\Omega_s^c}\left[\lambda n_\beta\phi_{,\gamma}{}^a(\mathbf{x})+\mu n_\alpha\delta_{\gamma\beta}\phi^a_{,\alpha}(\mathbf{x})+\mu n_\gamma\phi_{,\beta}{}^a(\mathbf{x})\right]d\Gamma\right\}+\\ &+\mathrm{i}k_z\sum_{a=1}^{N}\hat{u}_3^a\left(k_z,\omega\right)\int_{\partial\Omega_s^c}\lambda n_\beta\phi^a(\mathbf{x})d\Gamma+\sum_{a=1}^{N}\hat{u}_\beta^a(\omega)\int_{\Omega_s^c}\left[\omega^2\rho-\mu\left(k_z\right)^2\right]\phi^a(\mathbf{x})d\Omega+\\ &+\mathrm{i}k_z\sum_{a=1}^{N}\hat{u}_3^a\left(k_z,\omega\right)\int_{\Omega_s^c}\mu\phi^a_{,\beta}(\mathbf{x})d\Omega=0\end{aligned} \tag{27}$$

$$\begin{aligned}&\mathrm{i}k_z\sum_{a=1}^{N}\hat{u}_\alpha{}^a\left(k_z,\omega\right)\int_{\partial\Omega_s^c}\mu n_\alpha\phi^a(\mathbf{x})d\Gamma+\sum_{a=1}^{N}\hat{u}_3{}^a\left(k_z,\omega\right)\int_{\partial\Omega_s^c}\mu n_\alpha\phi^a_{,\alpha}(\mathbf{x})d\Gamma+\\ &+\mathrm{i}k_z\sum_{a=1}^{N}\hat{u}_\gamma^a\left(k_z,\omega\right)\int_{\Omega_s^c}\lambda\phi^a_{,\gamma}(\mathbf{x})d\Omega+\sum_{a=1}^{N}\hat{u}_3^a\left(k_z,\omega\right)\int_{\Omega_s^c}\left[\omega^2\rho-\left(k_z\right)^2\left(\lambda+2\mu\right)\right]\phi^a(\mathbf{x})d\Omega=0\end{aligned} \tag{28}$$

Eqs. (27, 28) are applied to all interior nodes $\mathbf{x}^c, (c=1,2,...,N_{in})$ located inside the domain Ω_2 and surrounded by the subdomain $\Omega_s^c \subset \Omega_2$, leading to $3N_{in}$ equations. The BEM approach is used for the nodes on the boundary. Boundary elements with one node at the center of the element are used. These nodes are also used for the MLS approximations (24) and (25).

3.2.2 Coupled BEM-MLPG formulation for interface Γ_2

This section describes how the mutual coupling of the BEM and the MLPG is formulated to obtain the elastic wave field generated by a dynamic load. This approach exploits a direct coupling between the BEM and MLPG. It can be done when the nodes used by the BEM match the nodes used by the MLPG. If the boundary nodes coincide, then the continuity of displacements and the equilibrium of tractions can be imposed directly.

The following coupling conditions should be considered on the mutual interface, Γ_2:

$$ {}^2\tilde{u}_i(\mathbf{x},k_z,\omega) = {}^3\tilde{u}_i(\mathbf{x},k_z,\omega),\ {}^2\tilde{t}_i(\mathbf{x},k_z,\omega) + {}^3\tilde{t}_i(\mathbf{x},k_z,\omega) = 0 \tag{29} $$

which should be valid at any point on the interface $\Gamma_2 = \partial\Omega_3$. The association of boundary densities to domains Ω_2 and Ω_3 is denoted by the left superscripts 2 and 3, respectively. The problem in the domain Ω_2 is described using the MLPG, while in the domain Ω_3 it is simulated using the BEM.

The displacement and traction fields at the interface Γ_2 can be approximated using the MLS approximations (24) and (25). The tractions are then given as:

$$ \begin{aligned} {}^2\tilde{t}_\beta(\mathbf{x},k_z,\omega) = &-{}^2\lambda(\mathbf{x})n_\beta(\mathbf{x})\mathrm{i}k_z\sum_{a=1}^{N}\hat{u}_3{}^a(k_z,\omega)\phi^a(\mathbf{x}) - \\ &- n_\alpha(\mathbf{x})\sum_{a=1}^{N}\hat{u}_\gamma{}^a(k_z,\omega)\left\{\delta_{\alpha\beta}\,{}^2\lambda(\mathbf{x})\phi_{,\gamma}{}^a(\mathbf{x}) + {}^2\mu(\mathbf{x})\left[\delta_{\beta\gamma}\phi_{,\alpha}{}^a(\mathbf{x}) + \delta_{\alpha\gamma}\phi_{,\beta}{}^a(\mathbf{x})\right]\right\} \end{aligned} \tag{30} $$

$$ {}^2\tilde{t}_3(\mathbf{x},k_z,\omega) = -{}^2\mu(\mathbf{x})n_\alpha(\mathbf{x})\sum_{a=1}^{N}\left[\hat{u}_\alpha{}^a(k_z,\omega)\mathrm{i}k_z\phi^a(\mathbf{x}) + \hat{u}_3{}^a(k_z,\omega)\phi_{,\alpha}{}^a(\mathbf{x})\right] \tag{31} $$

where the unit normal vector $\mathbf{n}(\mathbf{x})$ at $\mathbf{x}\in\Gamma_2$ is taken to be outward from the point of view of the domain Ω_3.

The mutual direct coupling between the BEM and the MLPG is accomplished by inserting the coupling conditions (29) into the boundary integral equation (12), which leads to:

$$ \begin{aligned} &p_{ij}\tilde{u}_i(\mathbf{x}_0,k_z,\omega) = -\int_{\Gamma_2}{}^2\tilde{t}_j(\mathbf{x},\mathbf{n}_n,k_z,\omega)G_{ij}(\mathbf{x},\mathbf{x}_0,k_z,\omega)\,d\Gamma - \\ &-\int_{\Gamma_2}{}^2\tilde{u}_j(\mathbf{x},k_z,\omega)H_{ij}(\mathbf{x},\mathbf{x}_0,\mathbf{n}_n,k_z,\omega)\,d\Gamma + \tilde{u}_i^{inc}(\mathbf{x}_0,\mathbf{x}_s,k_z,\omega) \end{aligned} \tag{32} $$

Finally, the numerical solution of Eq. (32) involves discretizing the boundary Γ_2 into a set of N_{be}^2 boundary elements Γ_q with constant approximation of boundary densities, leading to:

$$p_{ij}\tilde{u}_j\left(\mathbf{x}_0,k_z,\omega\right)=-\sum_{q=1}^{N_{be}^2}{}^2\tilde{t}_j\left(\mathbf{x}^q,k_z,\omega\right)\int_{\Gamma_q}G_{ij}\left(\mathbf{x},\mathbf{x}_0,k_z,\omega\right)d\Gamma_q- \\ -\sum_{q=1}^{N_{be}^2}{}^2\tilde{u}_j\left(\mathbf{x}^q,k_z,\omega\right)\int_{\Gamma_q}H_{ij}\left(\mathbf{x},\mathbf{x}_0,\mathbf{n}_n,k_z,\omega\right)d\Gamma_q+\tilde{u}_i^{inc}\left(\mathbf{x}_0,\mathbf{x}_s,k_z,\omega\right) \quad . \tag{33}$$

Taking into account Eq. (33) at nodal points on the interface $\Gamma_2 \ni \mathbf{x}^l \in \left\{\mathbf{x}^q\right\}_{q=1}^{N_{be}^2}$ with $N_{be}^2=N^{\Gamma_2}$, we obtain the set of discretized boundary integral equations:

$$p_{ij}\,{}^2\tilde{u}_j\left(\mathbf{x}^l,k_z,\omega\right)=-\sum_{q=1}^{N_{be}^2}{}^2\tilde{t}_j\left(\mathbf{x}^q,k_z,\omega\right)\int_{\Gamma_q}G_{ij}\left(\mathbf{x},\mathbf{x}^l,k_z,\omega\right)d\Gamma_q- \\ -\sum_{q=1}^{N_{be}^2}{}^2\tilde{u}_j\left(\mathbf{x}^q,k_z,\omega\right)\int_{\Gamma_q}H_{ij}\left(\mathbf{x},\mathbf{x}^l,\mathbf{n}_n,k_z,\omega\right)d\Gamma_q+\tilde{u}_i^{inc}\left(\mathbf{x}^l,\mathbf{x}_s,k_z,\omega\right) \quad . \tag{34}$$

which replace the boundary conditions at nodal points on $\partial\Omega_2\cap\Gamma_2$ in the numerical treatment of the problem in Ω_2 by the MLPG. The boundary densities ${}^2\tilde{u}_j$ and ${}^2\tilde{t}_\beta$, ${}^2\tilde{t}_3$ at the boundary nodes $\mathbf{x}^q$, $(q=1,...,N_{be}^2)$ are expressed according to Eqs. (24) and (30), (31), respectively, in terms of nodal unknowns $\hat{u}_i^a\left(k_z,\omega\right)$ used in the numerical solution in Ω_2 by the MLPG.

3.2.3 Coupled BEM-MLPG formulation for interface Γ_1

At any point $\mathbf{x}$ on the interface $\Gamma_1=\partial\Omega_1$ we must impose four boundary conditions between the solid and fluid: continuity of normal stresses and displacements and null shear stress.

$${}^2\tilde{u}_\beta(\mathbf{x},k_z,\omega)n_\beta(\mathbf{x})=\tilde{u}_{nf}(\mathbf{x},k_z,\omega),\ {}^2\tilde{t}_\beta(\mathbf{x},k_z,\omega)n_\beta(\mathbf{x})+\tilde{p}(\mathbf{x},k_z,\omega)=0 \tag{35}$$

$${}^2\tilde{t}_t(\mathbf{x},k_z,\omega)=-{}^2\tilde{t}_1(\mathbf{x},k_z,\omega)n_2(\mathbf{x})+{}^2\tilde{t}_2(\mathbf{x},k_z,\omega)n_1(\mathbf{x})=0 \tag{36}$$

$${}^2\tilde{t}_3(\mathbf{x},k_z,\omega)=0\,. \tag{37}$$

The procedure is the same as in the previous section. The displacement and traction fields at the interface Γ_1 can be approximated using the MLS approximations (24) and Eqs. (30), (31) with the unit normal vector $\mathbf{n}(\mathbf{x})$ at $\mathbf{x}\in\Gamma_1$ now being considered as outward from the point of view of the domain Ω_1. The numerical solution of Eq. (13) together with (35) involves discretizing the boundary Γ_1 into a set of N_{be}^1 ($N^{\Gamma_1}=N_{be}^1$) boundary elements, leading to:

$$c\tilde{p}\left(\mathbf{x}_0,k_z,\omega\right)=-\rho_1\omega^2\sum_{q=1}^{N_{be}^1}{}^2\tilde{u}_\beta\left(\mathbf{x}^q,k_z,\omega\right)n_\beta\left(\mathbf{x}^q\right)\int_{\Gamma_q}G_f\left(\mathbf{x},\mathbf{x}_0,k_z,\omega\right)d\Gamma-$$
$$-\sum_{q=1}^{N_{be}^1}{}^2\tilde{t}_\beta\left(\mathbf{x}^q,k_z,\omega\right)n_\beta\left(\mathbf{x}^q\right)\int_{\Gamma_q}H_f\left(\mathbf{x},\mathbf{x}_0,\mathbf{n}_n,k_z,\omega\right)d\Gamma \tag{38}$$

Taking into account Eqs. (36)-(38) at nodal points $\mathbf{x}^j\in\left\{\mathbf{x}^q\right\}_{q=1}^{N_{be}^1}$ on the interface Γ_1 with $N_{be}^1=N^{\Gamma_1}$, we obtain the set of discretized equations:

$${}^2\tilde{t}_1(\mathbf{x}^j,k_z,\omega)n_2(\mathbf{x}^j)-{}^2\tilde{t}_2(\mathbf{x}^j,k_z,\omega)n_1(\mathbf{x}^j)=0 \tag{39}$$

$${}^2\tilde{t}_3(\mathbf{x}^j,k_z,\omega)=0 \tag{40}$$

$$cn_\beta\left(\mathbf{x}^j\right){}^2\tilde{t}_\beta\left(\mathbf{x}^j,k_z,\omega\right)=\rho_1\omega^2\sum_{q=1}^{N_{be}^1}{}^2\tilde{u}_\beta\left(\mathbf{x}^q,k_z,\omega\right)n_\beta\left(\mathbf{x}^q\right)\int_{\Gamma_q}G_f\left(\mathbf{x},\mathbf{x}^j,k_z,\omega\right)d\Gamma+$$
$$+\sum_{q=1}^{N_{be}^1}{}^2\tilde{t}_\beta\left(\mathbf{x}^q,k_z,\omega\right)n_\beta\left(\mathbf{x}^q\right)\int_{\Gamma_q}H_f\left(\mathbf{x},\mathbf{x}^j,\mathbf{n}_n,k_z,\omega\right)d\Gamma \tag{41}$$

which replace the boundary conditions at nodal points on $\partial\Omega_2\cap\Gamma_1$ in the numerical treatment of the problem in Ω_2 by the MLPG. The boundary densities ${}^2\tilde{u}_j$ and ${}^2\tilde{t}_\beta$, ${}^2\tilde{t}_3$ at the boundary nodes $\mathbf{x}^q$, $(q=1,...,N_{be}^1)$ are expressed according to (24) and (30), (31), respectively, in terms of the nodal unknowns $\hat{u}_i{}^a\left(k_z,\omega\right)$ used in the numerical solution in Ω_2 by the MLPG.

Finally, we have $3N_{in}$ equations given by Eqs. (27), (28), $3N_{be}^2$ equations given by Eq. (34), and $3N_{be}^1$ equations given by Eqs. (39)-(41) which should be solved for $3N_{total}=3\left(N_{in}+N_{be}^1+N_{be}^2\right)$ nodal unknowns $\hat{u}_i{}^a\left(k_z,\omega\right)$ distributed in $\Omega_2\cup(-\Gamma_1)\cup(-\Gamma_2)$. Note that these nodal unknowns are complex variables.

3.3. BEM – FEM

3.3.1 FEM formulation for domain Ω_2

The 2.5D solid FEM formulation is based on the virtual work principle [44]:

$$-\omega^2\int_{\Omega_2}\delta\mathbf{u}\left(\mathbf{x},k_z,\omega\right)\rho_2\mathbf{u}\left(\mathbf{x},k_z,\omega\right)d\Omega+\int_{\Omega_2}\delta\tilde{\boldsymbol{\varepsilon}}\left(\mathbf{x},k_z,\omega\right)\boldsymbol{\sigma}\left(\mathbf{x},k_z,\omega\right)d\Omega=$$
$$=\int_{\Omega_2}\delta\mathbf{u}\left(\mathbf{x},k_z,\omega\right)\rho_2\mathbf{b}\left(\mathbf{x},k_z,\omega\right)d\Omega+\int_{\Gamma_2}\delta\mathbf{u}\left(\mathbf{x},k_z,\omega\right)\mathbf{q}\left(\mathbf{x},k_z,\omega\right)d\Gamma+$$
$$\int_{\Gamma_1}\delta\mathbf{u}\left(\mathbf{x},k_z,\omega\right)\mathbf{q}\left(\mathbf{x},k_z,\omega\right)d\Gamma \tag{42}$$

where $\mathbf{u}$ is the displacement vector, $\tilde{\boldsymbol{\varepsilon}}$ and $\boldsymbol{\sigma}$ are respectively the strain and stress tensors, $\rho_2\mathbf{b}$ is the body force and $\mathbf{q}$ is the traction at the boundaries, Γ_1 and Γ_2. A variable preceded by δ denotes a virtual change of this magnitude.

Once the displacements at the cross section of Ω_2 are approximated within element interpolation shape functions, the stress and strain vectors are derived from displacements through the constitutive law of material, assuming linear behavior and a homogeneous medium. The spatial derivatives involved in the strain-displacement relation are solved by means of a Fourier transform, as described in the previous section.

After these procedures, Equation (42) is written as [45]:

$$\left[-\omega^2\mathbf{M}+\mathbf{K}^0-ik_z\mathbf{K}^1+k_z^2\mathbf{K}^2\right]\tilde{\mathbf{u}}\left(\mathbf{x},k_z,\omega\right)=\tilde{\mathbf{f}}\left(\mathbf{x},k_z,\omega\right) \tag{43}$$

where $\mathbf{M}$ is the mass matrix, $\mathbf{K}^0$, $\mathbf{K}^1$ and $\mathbf{K}^2$ are stiffness matrices, $\tilde{\mathbf{u}}$ is the nodal displacement, and $\tilde{\mathbf{f}}$ is the external force. The meanings of these matrices are well established in References [44-46]. The FEM matrices are computed considering nonhomogeneous material properties.

Equation (43) is rewritten as shown below if an equivalent dynamic stiffness matrix, $\mathbf{D}$, is considered:

$$\mathbf{D}\left(k_z,\omega\right)\tilde{\mathbf{u}}\left(\mathbf{x},k_z,\omega\right)=\tilde{\mathbf{f}}\left(\mathbf{x},k_z,\omega\right) \tag{44}$$

3.3.2 Coupled BEM-FEM formulation for interfaces Γ_1 *and* Γ_2

Equations (12) and (44) are coupled when force equilibrium and displacement continuity are imposed at the interface Γ_2 as it was indicated in Section 3.2.2. Equations (13) and (44) are coupled by the equilibrium of normal pressure, null shear stresses and the compatibility of displacement at the interface Γ_1 as presented in Section 3.2.3. These equations are assembled into a single system [46].

4. Performance of the proposed numerical procedure

The performance comparison of the proposed model is verified by taking a nonhomogeneous elastic annular circular fluid filled borehole region, Ω_2, with an internal radius $r_{\text{int}}=0.75\,\text{m}$ and an external radius $r_{ext}=1.5\,\text{m}$, centered at $\left(x_{cen}=0.0\,\text{m};\,y_{cen}=0.0\,\text{m}\right)$ and buried in an unbounded homogeneous elastic medium, Ω_1. The system is excited by a blast line load whose amplitude may vary sinusoidally in the third dimension ($k_z=0.0\,\text{rad/m}$ and $k_z=2.0\,\text{rad/m}$), located at a given point $\left(x_0=-4.0\,\text{m};\,y_0=0.0\,\text{m}\right)$ in the outer homogeneous domain, as illustrated in Figure 3.

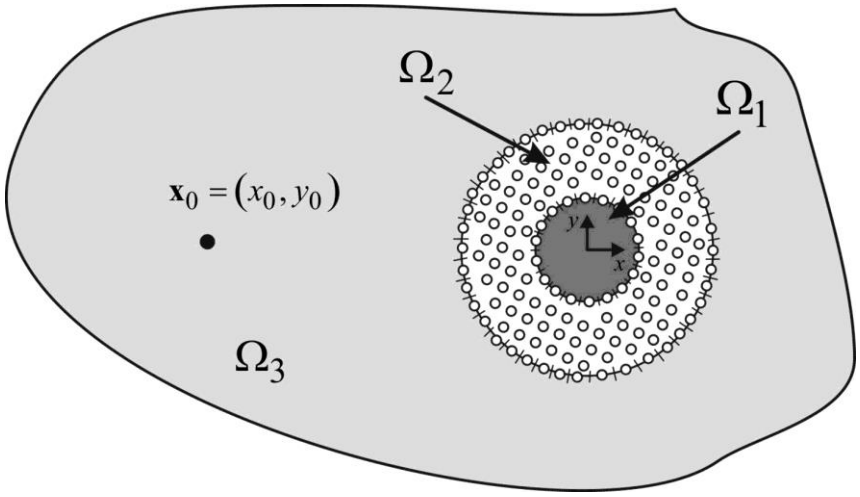

Figure 3: Geometry of the model used to verify the algorithm

The host medium, with an elasticity modulus of $E_0 = 11689288.6$ kPa, a Poisson ratio of 0.29593 and density of 2140 kg/m^3, allows P and S wave velocities of 2696.5 m/s and 1451.7 m/s, respectively. Inside the nonhomogeneous circular annular region the density of 2500 kg/m^3 and the Poisson ratio of 0.15 are assumed to be constant. However, a radial variation of the elasticity modulus is assumed as follows,

$$E(r) = E_1 + \frac{(E_0 - E_1)}{2}\left[1 + \cos\left(\pi \frac{(r_d - r_{\text{int}})}{r_{\text{int}}} - \pi\right)\right], \tag{50}$$

with $E_1 = 28980000.0$ kPa and $r_d = \sqrt{(x - x_{cen})^2 + (y - y_{cen})^2}$ (see Figure 4).

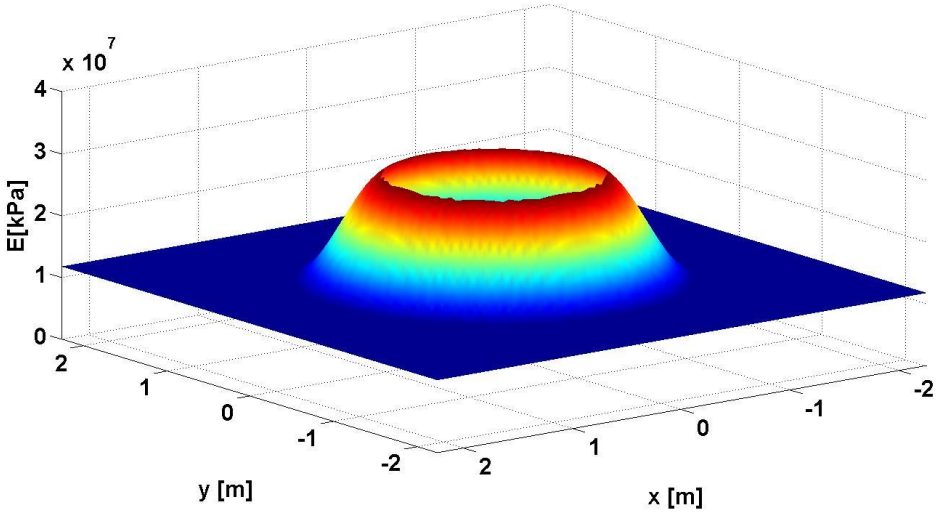

Figure 4: Elasticity modulus variation.

Thus, the annular medium allows P-wave and S-wave velocities in the close vicinity of the fluid borehole wall of $3498.6\,\mathrm{m/s}$ and $2244.9\,\mathrm{m/s}$, respectively. The fluid medium, Ω_1, is water with a density of $1000\ \mathrm{kg/m^3}$ that allows P-wave velocities of $1500.0\,\mathrm{m/s}$

The system is loaded by the incident field source located at $\mathbf{x}_0 = (x_0, y_0)$, which is given as:

$$u_x^{inc}(\mathbf{x}_0, \mathbf{x}_s, k_z, \omega) = \frac{\mathrm{i}}{2} k_{c_p} H_1\left(k_{c_p} r\right) \frac{\partial r}{\partial x}$$

$$u_y^{inc}(\mathbf{x}_0, \mathbf{x}_s, k_z, \omega) = \frac{\mathrm{i}}{2} k_{c_p} H_1\left(k_{c_p} r\right) \frac{\partial r}{\partial y} \tag{51}$$

$$u_z^{inc}(\mathbf{x}_0, \mathbf{x}_s, k_z, \omega) = \frac{k_z}{2} H_0\left(k_{c_p} r\right)$$

with $r = \sqrt{(\mathrm{x}_0 - \mathrm{x}_s)^2 + (\mathrm{y}_0 - y_s)^2}$ and $k_{c_p} = \sqrt{\omega^2 / c_p{}^2 - k_z^2}$, assuming $\mathrm{Im}\left(k_{c_p}\right) < 0$. The analytical solution of this system can be found in Tadeu et al. [39].

The pressure and displacement fields generated by harmonic sources with frequencies of 500.0 Hz, 1000.0 Hz and 4000.0 Hz were used to verify the performance of both the coupled BEM-MLPG and BEM-FEM approaches. The convergence was studied using different nodal mesh densities. The limiting interfaces Γ_1 and Γ_2 within the unbounded fluid subdomain and the solid subdomain, respectively, were represented with N_{be}^1 and N_{be}^2 ($N_{be}^2 = N_{be}^1$) boundary elements.

The MLPG nodes were distributed evenly on a number of radii $N_r = N_{be}^1 (r_{ext} - r_{\mathrm{int}}) / (2\pi r_{ext})$ according to the boundary nodes shown in Figure 5. The numerical MLPG calculations were performed using a radius of the local support domain (r^i) that was three times the nodal point distance ($3h$). This relation was found to provide the best results in a previous work by the authors [39]. Moreover, the computations with the FEM-BEM approach were done with a FEM discretization of the damaged solid subdomain Ω_2, which uses the same nodal distribution as the MLPG. In this way, both the structured quadrilateral and unstructured triangular meshes were obtained as shown in Figure 6. The problem solution was computed at the MLPG or FEM nodal points and over a grid of 5999 equally spaced receivers between ($-2.25\mathrm{m} \le x \le 2.25\mathrm{m}, -2.25\mathrm{m} \le y \le 2.25\mathrm{m}$) (5388 in the exterior solid media Ω_3 and 611 in the fluid medium Ω_1).

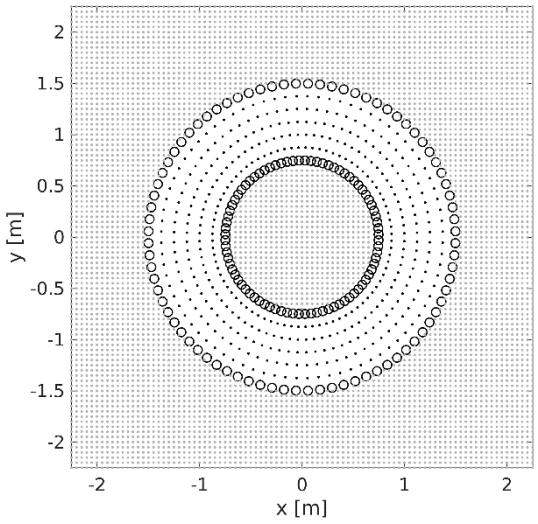

Figure 5: MLPG-BEM problem discretization: boundary nodes (circles), internal nodes (black points) and receivers grid (grey nodes) for $N_{be}^{1} = 80$.

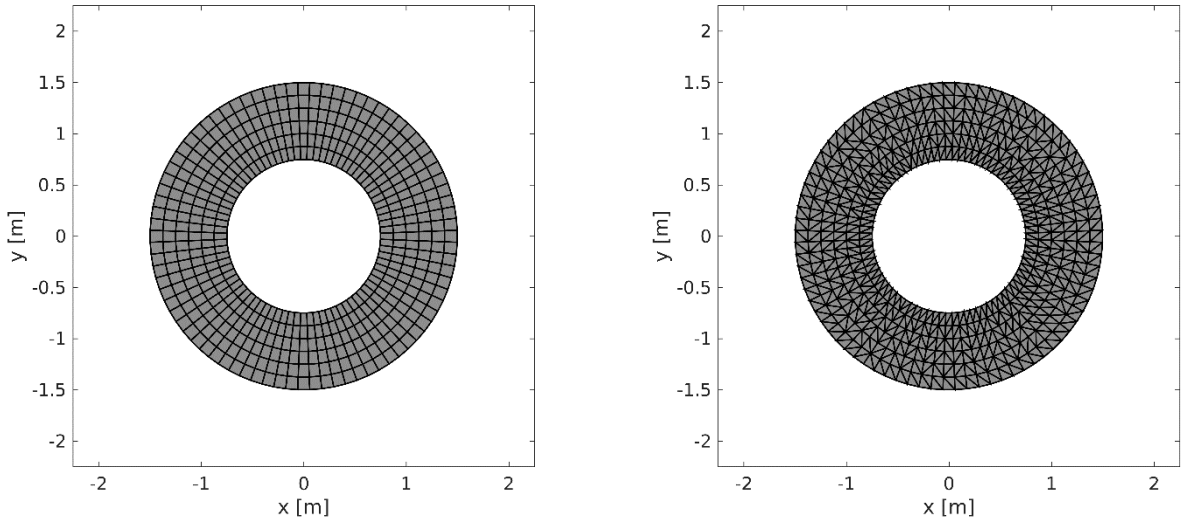

Figure 6: (a) Structured quadrilateral mesh and (b) unstructured triangular mesh for the FEM-BEM discretization with $N_{be}^{1} = 80$.

As the number of the nodal points influences the accuracy of the response, the external and the internal interfaces, Γ_1 and Γ_2, were discretized with a varying number of boundary elements, 80 to 200, while 400 to 2800 regularly distributed internal nodes were used. The number of the internal nodes was set so that the distance between them was the same as that between the boundary nodes. The error for each receiver is calculated as the difference

between the analytical and the numerical result. The global performance of the solution is assessed by the normalized average error, computed in the solid media and fluid medium as follows:

$$\overline{error_{u_i}} = \frac{\frac{1}{N_{rec_{sol}}} \sum_{n=1}^{Nrec_{sol}} \left| u_i\left(\mathbf{x}, k_z, \omega\right) - \hat{u}_i\left(\mathbf{x}, k_z, \omega\right) \right|}{\left| u_{i,\max}\left(\mathbf{x}, k_z, \omega\right) \right|},$$

$$\overline{error_p} = \frac{\frac{1}{N_{rec_{fl}}} \sum_{n=1}^{Nrec_{fl}} \left| p\left(\mathbf{x}, k_z, \omega\right) - \hat{p}\left(\mathbf{x}, k_z, \omega\right) \right|}{\left| p_{\max}\left(\mathbf{x}, k_z, \omega\right) \right|} \tag{52}$$

where $u_i\left(\mathbf{x}, k_z, \omega\right)$ and $p\left(\mathbf{x}, k_z, \omega\right)$ are the analytical displacements and pressure solutions; $\left|u_{i,\max}\left(\mathbf{x}, k_z, \omega\right)\right|$ and $\left|p_{\max}\left(\mathbf{x}, k_z, \omega\right)\right|$ are the maximum absolute response over the grid of receivers; $\hat{u}_i\left(\mathbf{x}, k_z, \omega\right)$ and $\hat{p}\left(\mathbf{x}, k_z, \omega\right)$ are the numerical results.

Figures 7 and 8 illustrate the average normalized errors when structured quadrilateral FEM meshes were used, while Figures 9 and 10 display the results provided in the presence of unstructured triangular FEM meshes. A logarithmic scale is used to enhance the average amplitude errors. As expected, the analysis of the results shows that the error is higher at higher frequencies, and in general decreases as the number of nodes increases.

Figure 7 displays the average normalized errors of the numerical solution for $k_z = 0.0$ rad/m. The analysis of the fluid pressure results (Figure 7a) shows that at 4000.0 Hz and for a lower number of nodes the best results are provided by the BEM-MLPG coupling model. As the number of nodes increases the BEM-FEM coupling model tends to ensure better results. For 500.0 Hz and 1000.0 Hz, the BEM-FEM coupling model provides the best results for the full range of nodes. When we move from $k_z = 0.0$ rad/m to $k_z = 2.0$ rad/m (Figure 8a) it can be seen that the pressure results retain the same behavior at 4000.0 Hz. For excitation frequencies of 500.0 Hz and 1000.0 Hz, the best results are provided by the BEM-FEM coupling model. However, the BEM-FEM convergence is poor for the frequency of 500.0 Hz when a higher number of nodes are used because the coupled system of equations becomes ill-conditioned. Analyzing the average normalized displacement errors, it can be concluded that for $k_z = 0.0$ rad/m the best results tend to be provided by the BEM-MLPG model. For $k_z = 2.0$ rad/m, the BEM-FEM model exceeds the BEM-MLPG results at 500.0 Hz and 1000.0 Hz, particularly when a smaller number of nodes are used. At 4000.0 Hz the best results are provided by the BEM-MLPG model. It should be noted that the convergence of the BEM-FEM does not exhibit a monotonic decrease of the error. A minimum error is reached for a certain number of nodes and the problem is poorly approximated due to numerical error for finer discretization.

The use of unstructured triangular FEM meshes leads to similar behavior (see Figures 9 and 10) to that found for structured quadrilateral FEM meshes. However the pressure results obtained for a frequency of excitation of 4000.0 Hz by the BEM-FEM coupling model come out best when very few nodes are used for both $k_z = 0.0\,\text{rad/m}$ and $k_z = 2.0\,\text{rad/m}$. As the number the nodes increases, the BEM-MLPG leads to the best results. The displacement results obtained in the solid media and generated by a high frequency of excitation (4000.0 Hz) are better when computed by the BEM-MLPG coupling model.

Comparing the BEM-FEM results provided from both kinds of meshes it can be concluded that the problem approximation with structured quadrilateral meshes presented an error slightly lower than that for unstructured triangular discretization. In both cases, the errors have similar behavior. However, unstructured triangular meshes could be desirable from time to time when the discretization does not allow a structured quadrilateral mesh.

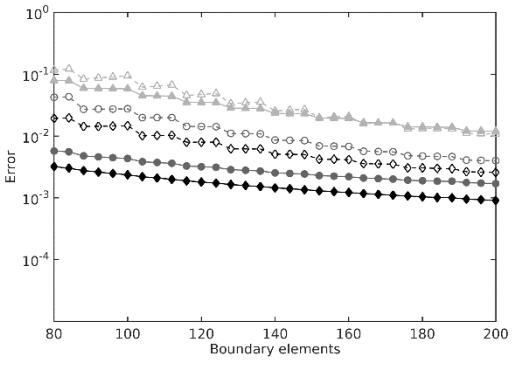

a)

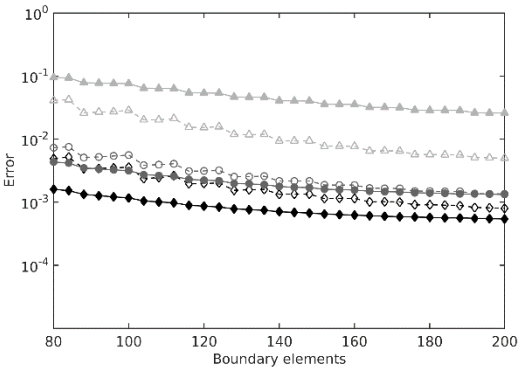

b)

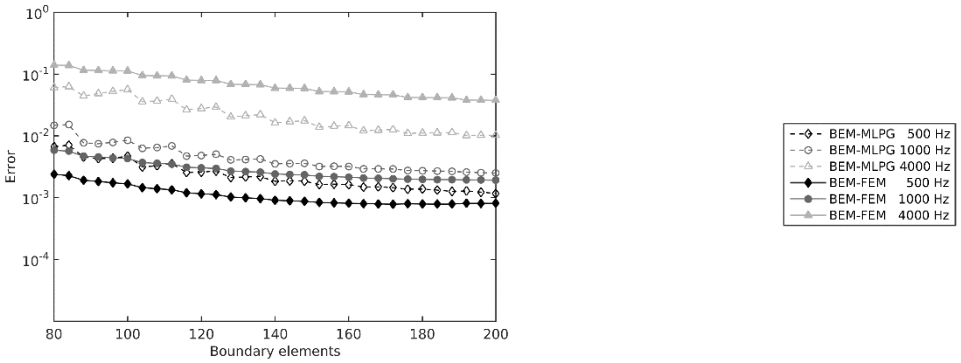

c)

Figure 7: Average normalized errors of the numerical solution for a harmonic source at frequencies of $500.0\,\text{Hz}$, $1000.0\,\text{Hz}$ and $4000.0\,\text{Hz}$, with wavenumbers $k_z = 0.0\,\text{rad/m}$, when structured quadrilateral FEM meshes are used: a) fluid pressure; b) u_x displacements; c) u_y displacements.

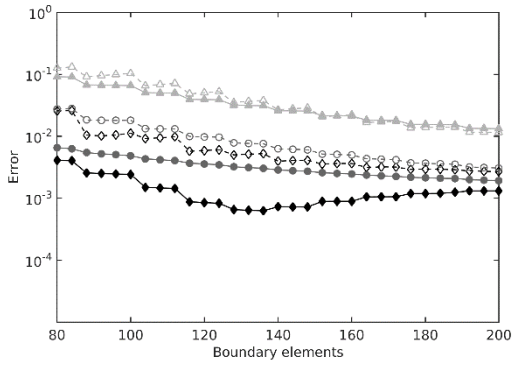

a)

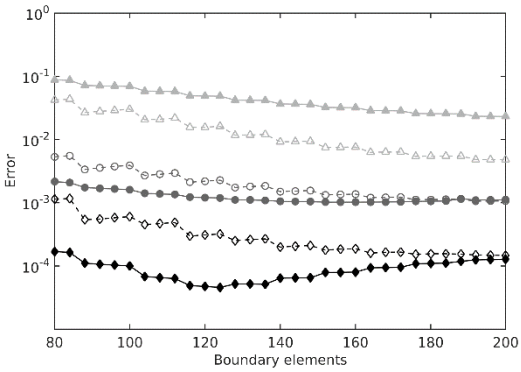

b)

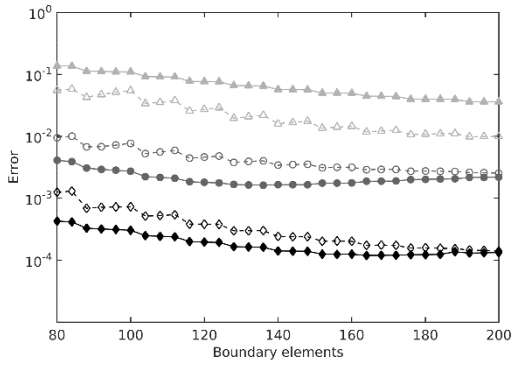

c)

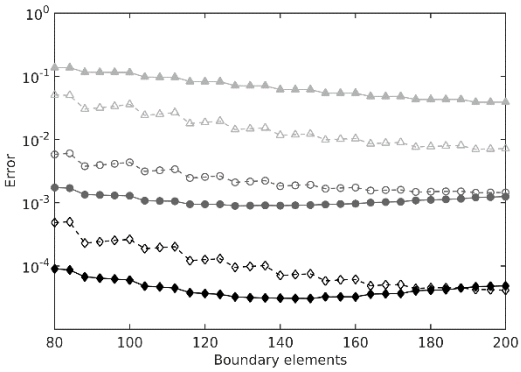

d)

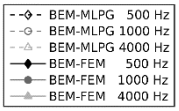

Figure 8: Average normalized errors of the numerical solution for a harmonic source at frequencies of $500.0\,\text{Hz}$, $1000.0\,\text{Hz}$ and $4000.0\,\text{Hz}$, with wavenumbers $k_z = 2.0\,\text{rad/m}$, when structured quadrilateral FEM meshes are used: a) fluid pressure; b) u_x displacements; c) u_y displacements; d) u_z displacements.

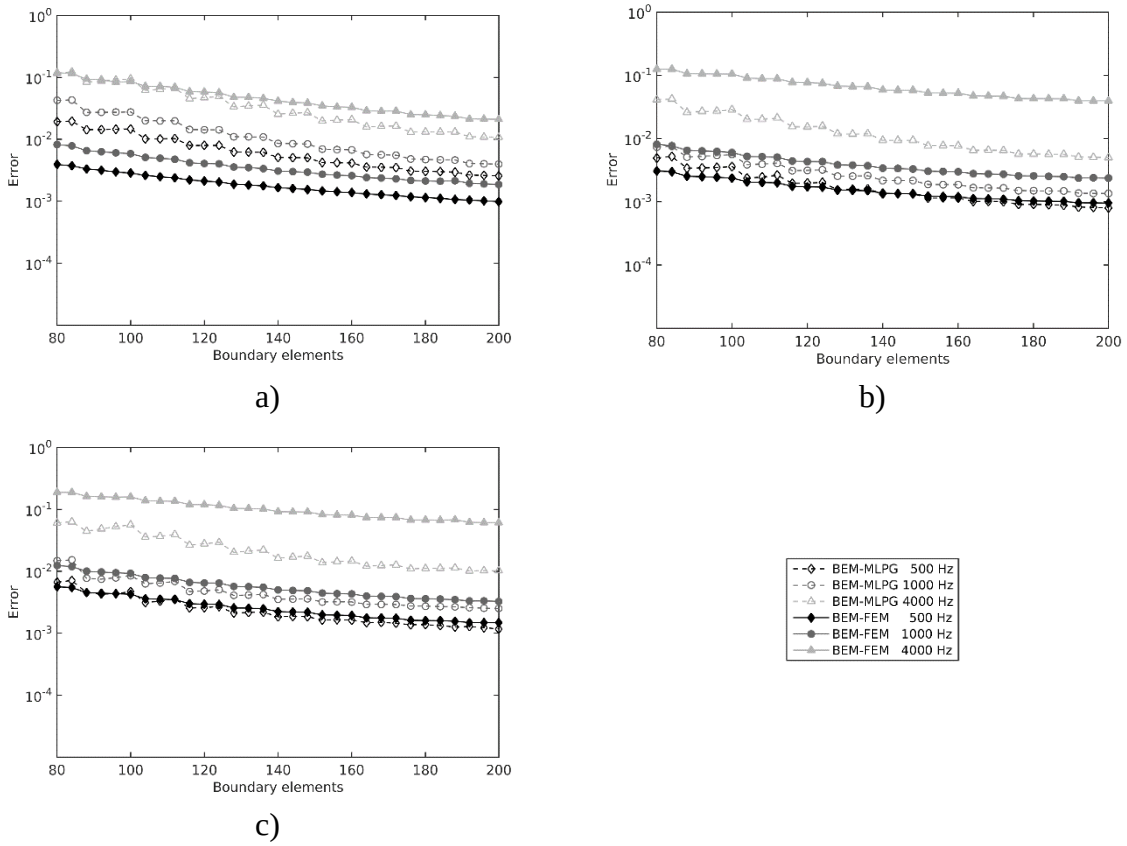

Figure 9: Average normalized errors of the numerical solution for a harmonic source at frequencies of $500.0\,\text{Hz}$, $1000.0\,\text{Hz}$ and $4000.0\,\text{Hz}$, with wavenumbers $k_z = 0.0\,\text{rad/m}$, when unstructured triangular FEM meshes are used: a) fluid pressure; b) u_x displacements; c) u_y displacements.

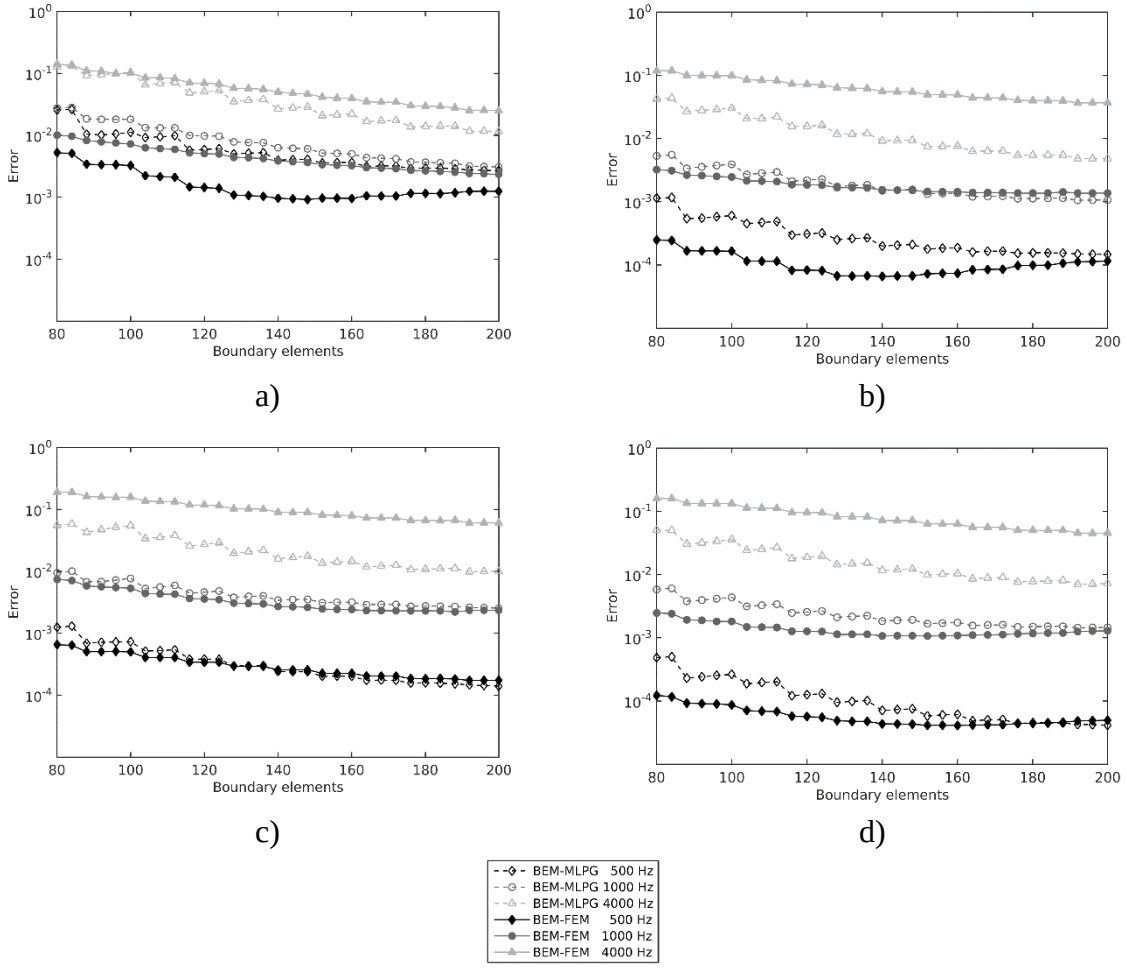

Figure 10: Average normalized errors of the numerical solution for a harmonic source at frequencies of $500.0\,\text{Hz}$, $1000.0\,\text{Hz}$ and $4000.0\,\text{Hz}$, with wavenumbers $k_z = 2.0\,\text{rad/m}$, when unstructured triangular FEM meshes are used: a) fluid pressure; b) u_x displacements; c) u_y displacements; d) u_z displacements.

5. Conclusions

This paper compares the efficiency of two different coupling formulations (the boundary element method (BEM) - meshless local Petrov-Galerkin (MLPG) and the BEM- finite

element method (FEM)) used to simulate the propagation of elastic and pressure waves in fluid-filled boreholes with damaged, nonhomogeneous, bounded media, when subjected to the field generated by a 2.5D blast source. The BEM was used to simulate the wave propagation in the outer medium and the inner fluid-filled domain, while the MLPG and the FEM were used to model the localized regions with nonhomogeneous properties, for which the BEM is not suitable. Structured quadrilateral and unstructured triangular FEM meshes were both used. A detailed formulation description of the two models in the frequency domain has been provided. The efficiency of the proposed coupling formulations consists in localization of unknowns to nodal points in the domain with nonhomogeneous properties and its boundary. The boundary integral equations from homogeneous subdomains play the role of un-prescribed boundary conditions on interfaces.

The performance of each coupled model was assessed using a circular multi-layered system to simulate the damaged zone, for which analytical solutions are known. The results confirmed the suitability of both models, for different frequencies and axial wavenumbers. It was found that in general the BEM-MLPG model led to better results than the BEM-FEM at high frequencies of excitation.

Although the BEM-FEM discretisations based on unstructured meshes gave good approximations, the BEM-MLPG would be much suitable to overcome the difficulties to represent irregular domains due to the inherent advantages of the meshless method.

6. Acknowledgements

The research work presented herein was supported by the project POCI-01-0247-FEDER-003474, funded by Portugal 2020 through the Operational Programme for Competitiveness Factors (COMPETE 2020). This work was also supported by the Spanish Ministry of Economy and Competitiveness (Ministerio de Economía y Competitividad) under the research project [BIA2013-43085-P]. The authors also wish to acknowledge the support provided by the Andalusian Scientific Computing Centre (CICA). Finally the support by the Slovak grant agency VEGA under the project VEGA 2/0046/16 is acknowledged.

7. References

[1] Aliabadi MH, editor. (2002) The boundary element method: applications in solids and structures. Wiley.

[2] Tadeu A., Kausel E., Vrettos C. (1996) Scattering of waves by subterranean structures via the boundary element method. Soil Dyn Earthquake Eng; 15(6): pp. 387–97.

[3] Liu E, Zhang Z. (2001) Numerical study of elastic wave scattering by cracks or inclusions using the boundary integral equation method. Journal of Computational Acoustics; 9(3):1039–54.

[4] Thompson L.L. (2006) A review of finite-element methods for time-harmonic acoustics. J Acoust Soc Am; 119(3): pp. 1315–30.

[5] Zhang C., Zhao C. (1987) Coupling method of finite and infinite elements for strip foundation wave problems. Earthquake Engineering and Structural Dynamics; 15: pp. 839– 851.
[6] Han X., Liu G.R., Xi Z.C., Lam K.Y. (2001) Transient waves in a functionally graded cylinder. International Journal of Solids and Structures; 38: pp. 3021–37.
[7] Atluri S.N. (2004) The meshless method (MLPG) for domain & BIE discretizations. Tech. Science Press.
[8] Sladek J., Sladek V., VanKeer R. (2003) Meshless local boundary integral equation method for 2D elastodynamic problems. International Journal for Numerical Methods in Engineering; 57: pp. 235–49.
[9] Hosseini SM. (2012) Analysis of elastic wave propagation in a functionally graded thick hollow cylinder using a hybrid mesh-free method, Engineering Analysis with Boundary Elements; 36: pp. 1536–45.
[10] Gu Y.T., Liu G.R. (2005) Meshless Methods Coupled with Other Numerical Methods. Tsinghua Science & Technology; 10: pp. 8 – 10.
[11] Irons, B. M., Razzaque, A. (1972) Experience with the patch test for convergence of finite element method. In: The Mathematics of Finite Elements with Application to Partial Differential Equations (Aziz, A. R. (Ed.)), Academic Pres USA, p. 557–587.
[12] Taylor, R.L., Simo, J.C., Zienkiewicz, O.C., Chan, A.C.H. (1986) The patch test—a condition for assessing FEM convergence. International Journal for Numerical Methods in Engineering. 22, 1, pp. 39–62.
[13] Schmidt, G., Strese, H. (1989) The convergence of a direct BEM for the plane mixed boundary value problem of the Laplacian. Numerische Mathematik, 57, 2, pp. 145-165.
[14] Vavourakis, V.; Sellountos, E. J.; Polyzos, D. (2006) A comparison study on different MLPG (LBIE) formulations. CMES: Computer Modeling in Engineering & Sciences, vol. 13, No. 3, pp. 171-183.
[15] Augarde, C. E.; Deeks, A. J. (2005) On the effects of nodal distributions for imposition of essential boundary conditions in the MLPG meshfree method. Communications in Numerical Methods in Engineering, vol. 21, pp. 389–395.
[16] Sladek, V., Sladek, J., Zhang, C. (2006) A Comparative Study of Meshless Approximations in Local Integral Equation Method. CMC – Computers, Materials and Continua, 4, 3, pp.177-188.
[17] Sladek J., Stanak P., Han Z. D., Sladek V., Atluri S. N. (2013) Applications of the MLPG Method in Engineering & Sciences: A Review. CMES: Computer Modeling in Engineering & Sciences; 92(5), pp. 423-475.
[18] Liu G. R., Gu Y. T. (2000) Meshless local Petrov-Galerkin (MLPG) method in combination with finite element and boundary element approaches. Computational Mechanics; 26, pp. 536-546.
[19] Chen T., Raju I.S. (2003) A coupled finite element and meshless local Petrov-Galerkin method for two-dimensional potential problems. Computer Methods in Applied Mechanics and Engineering; 192, pp. 4533 – 4550.

[20] Zhao M., Nie Y. (2008) A Study of Boundary Conditions in the Meshless Local Petrov-Galerkin (MLPG) Method for Electromagnetic Field Computations. CMES: Computer Modeling in Engineering & Sciences; 37(2): 97-112.

[21] Zienkiewicz OC, Kelly DM, Bettes P. (1977) The coupling of the finite element method and boundary solution procedures. Int J Numer Meth Eng; 11:355–76.

[22] Romero, A., Galvín, P. (2015) A BEM–FEM using layered half-space Green′s function in time domain for SSI analyses. Engineering Analysis with Boundary Elements, 55, pp. 93-103**.**

[23] Coulier P, François S, Lombaert G, Degrande G. (2014) Coupled finite element–hierarchical boundary element methods for dynamic soil–structure interaction in the frequency domain. Int J Numer Meth Eng; 97:505–30.

[24] Tadeu A., Simões N., Simões I. (2010) Coupling BEM/TBEM and MFS for the simulation of transient conduction heat transfer. Int J Numer Methods Eng; 84(2), pp. 179–213.

[25] Godinho L., Tadeu A. (2012) Acoustic analysis of heterogeneous domains coupling the BEM with Kansa's method. Eng. Anal. Bound. Elem.; 36: 1014-1026.

[26] Belytschko T., Organ D., Krongauz Y. (1995) Coupled finite element – element-free Galerkin method. Comput. Mech.; 17, pp. 186 – 195.

[27] Godinho, L., Amado-Mendes, P., Pereira, A., Soares Jr., D. (2013) A coupled MFS–FEM model for 2-D dynamic soil–structure interaction in the frequency domain. Computers & Structures, 129, pp. 74-85.

[28] Godinho, L., Amado-Mendes, P., Tadeu, A. (2015) Meshless analysis of soil–structure interaction using an MFS–MLPG coupled approach. Engineering Analysis with Boundary Elements, 55, pp. 80-92.

[29] Tadeu, A.; Stanak, P.; Sladek, J.; Sladek, V.; Prata, J.; Simões, N. A. (2013): Coupled BEM-MLPG Technique for the Thermal Analysis of Non-Homogeneous Media. CMES - Computer Modeling in Engineering & Sciences. vol. 93, No. 6, pp. 489-516.

[30] Tadeu, A.; Stanak, P.; Sladek, J.; Sladek, V. (2014): Coupled BEM–MLPG acoustic analysis for non-homogeneous media, Engineering Analysis with Boundary Elements. vol. 44, pp. 161-169.

[31] Tadeu, A.; Stanak, P.; Antonio, J.; Sladek, J.; Sladek, V. (2015): 2.5D Elastic wave propagation in non-homogeneous media coupling the BEM and MLPG methods. Engineering Analysis with Boundary Elements. vol. 53, pp. 86-99.

[32] Godinho, L., Soares Jr., D. (2013) Frequency domain analysis of interacting acoustic–elastodynamic models taking into account optimized iterative coupling of different numerical methods. Engineering Analysis with Boundary Elements, 37, 7–8, pp. 1074-1088.

[33] Wendland, W. L. (1988) On Asymptotic Error Estimates for Combined Bem and Fem. In: Stein, E. and Wendland, W. Finite Element and Boundary Element Techniques from Mathematical and Engineering Point of View, Vol. 301 of the series CISM International Centre for Mechanical Sciences. pp. 273-333.

[34] Randall, C.T. (1991) Multipole acoustic waveforms in nonaxisymmetric boreholes and formations. Journal of the Acoustical Society of America. 90, pp. 1620– 1631.

[35] Leslie, H.D., Randall, C.T. (1992) Multipole sources in boreholes penetrating anisotropic formations: numerical and experimental results. Journal of the Acoustical Society of America. 91, pp. 12– 27.

[36] Bouchon, M. (1993) A numerical simulation of the acoustic and elastic wavefields radiated by a source in a fluid-filled borehole embedded in a layered medium. Geophysics. 58, pp. 475–481.

[37] Cheng, N., Cheng, C.H., Toksoz, M.N. (1995) Borehole wave propagation in three dimensions. Journal of the Acoustical Society of America. 97, pp. 3483– 3493.

[38] Dong, W., Bouchon, M., Toksfz, M.N. (1995) Borehole seismic source radiation in layered isotropic and anisotropic media: boundary element modeling. Geophysics. 60, pp. 735– 747.

[39] Tadeu, A.; Stanak, P.; Antonio, J.; Sladek, J.; Sladek, V. (2015) The influence of non-homogeneous material properties on elastic wave propagation in fluid-filled boreholes. CMES - Computer Modeling in Engineering & Sciences. vol. 107, No. 5, pp. 345-378.

[40] Tadeu A., Kausel E. (2000) Green's functions for two-and-a-half-dimensional elastodynamic problems, ASCE J. Engrg. Mech.; 126(10), pp. 1093–1096.

[41] Tadeu, A.; Santos, P.F.A.; Kausel, E. (1999) Closed-Form Integration of Singular Terms for Constant, Linear and Quadratic Boundary Elements: Part I. SH Wave Propagation. Engineering Analysis with Boundary Elements. vol. 23, pp. 671–681.

[42] Tadeu, A.; Santos, P.F.A.; Kausel, E. (1999) Closed-form Integration of Singular Terms for Constant, Linear and Quadratic Boundary Elements: Part II. SV-P Wave Propagation. Engineering Analysis with Boundary Elements. vol. 23, pp. 757–768.

[43] Wen, P.H.; Aliabadi, M.H. (2008) An improved meshless collocation method for elastostatic and elastodynamic problems. Commun Num Meth Eng; vol. 24, pp. 635-651.

[44] Gavrić, L. (1994) Finite Element Computation of Dispersion Properties of Thin-Walled Waveguides. Journal of Sound and Vibration. vol. 173, pp. 113-124.

[45] François, S.; Schevenels, M.; Galvín, P.; Lombaert, G.; Degrande, G. (2010) A 2.5D coupled FE-BE methodology for the dynamic interaction between longitudinally invariant structures and a layered halfspace. Computer Methods in Applied Mechanics and Engineering. vol. 199, pp. 1536-1548.

[46] Gavrić, L. (1995) Computation of propagative waves in free rail using a finite element technique. Journal of Sound and Vibration. vol. 185, pp. 531-543.

[47] Romero, A.; Tadeu, A.; Galvín, P.; António, J. (2015) 2.5D coupled BEM-FEM used to model fluid and solid scattering wave. International Journal for Numerical Methods in Engineering. vol. 101, pp. 148-164.